Optimization Design of a V-shaped Flux Switching Permanent Magnet Traction motor for Railway Applications

Pattasad Seangwong[1,*] and Pirat Khunkitti[1]

[1] Department of Electrical Engineering, Faculty of Engineering, Khon Kaen University, Khon Kaen 40002, Thailand

*Corresponding Email : pattasad_s@kkumail.com

Received October 4, 2023, Revised November 12, 2023, Accepted November 16, 2023, Published February 8, 2024

Abstract. *This paper presents the optimization design of a V-shaped flux-switching permanent magnet motor (V-FSPM) for railway traction applications. The analysis of this V-FSPM involved employing 2-D FEM. Given the complexity of this motor's structure, to achieve accurate and efficient optimization, the comprehensive genetic design optimization method is utilized in this study. This method takes into consideration various sensitivity indices, incorporating design variable sensitivity analysis and genetic algorithm (GA) optimization. The results demonstrate a significant enhancement in the output torque with reduced torque ripple of the proposed V-FSPM motor. These enhancements collectively contribute to the advancement of a more dependable and efficient railway system.*

Keywords:

permanent magnet motor, railway traction applications, flux-switching, sensitivity analysis, genetic algorithm optimization

1. Introduction

Railways provide an efficient and sustainable transportation solution, remarkable in energy efficiency, pollution reduction, safety prioritization, congestion relief, and cost-effectiveness for passengers and freight. They offer reliability, long-distance travel comfort, and support environmental sustainability, making them an essential component of modern transportation systems. Electric traction stands out as the most efficient propulsion system for railways when compared to alternative solutions like classical steam propulsion and diesel-electric engines [1]. This approach offers numerous advantages, including reduced pollution, enhanced control flexibility, and quick start-stop capabilities. Over the last century, with advancements in electric drives for traction systems [2]-[3], railway electrification has emerged as a dominant choice among various rail operators [4]-[6].

Recent trends indicate that permanent magnet synchronous motors (PMSM) will play a significant role in future railway traction applications [7]-[8]. PMSMs offer high efficiency, an improved power-to-weight ratio (power density), and benefits like the elimination of field-excitation losses, increased efficiency, lower rotor inertia, and the ability to use regenerative brakes even at low speeds [9]-[11]. PMSMs can be categorized based on magnet arrangements, namely rotor permanent magnet machines (RPM) and stator permanent magnet machines (SPM). In particular, SPMs with magnets placed on the stator. They are notable for their low rotor inertia, and flux-focusing effect, resulting in a robust rotor structure, high power density, efficiency, and power factor [12]-[15]. Among SPMs, the flux-switching permanent magnet (FSPM) motor offers high power density [16], sinusoidal back electromotive force (EMF), and fault-tolerance capabilities [17], outperforming other SPM motors. These attributes make FSPM motors an appealing choice for direct-driven systems like railway transit.

FSPM has received a lot of attention recently due to its magnetic distribution and other advantages. Increasing the power density of FSPM motors for railway applications involves a number of techniques. In 2022, an FS transverse-flux PM linear motor was systematically designed to achieve larger thrust and reduced cogging force through a simple structure [18]. This method effectively minimized cogging force and increased thrust force, making it suitable for linear traction motors. Linear FS machines are designed for long-stroke applications. the reduction of thrust ripple has been a key focus. Through the application of additional pole optimization, the results of 2D Finite Element Method (FEM) analysis have demonstrated the superior performance of the novel design solutions presented in this study. These solutions are remarkable in minimizing both detent force and rated thrust ripple [19]. A segmented stator FS linear hybrid excited machine designed for electric power trains has undergone detailed design and analysis [20]. This machine's key design parameters were subjected to global optimization using a multi-objective genetic global optimization approach. This optimization process not only led to a reduction in the volume of PM but also resulted in an increase in thrust force and thrust density. A fault-tolerant field-excited linear FS machine featuring concentrated and toroidal windings designed for rail transportation systems underwent analysis and optimization [21]. Initial designs

were enhanced through the application of a genetic algorithm (GA), leading to a notable increase in average thrust force. However, these advancements come with limitations, including restricted slot area and the potential for increased power density. To address these challenges in conventional FSPM motors, a novel complementary and modular V-shaped FSPM motor was introduced. Utilizing V-shaped stator poles has become a popular technique for enhancing the electromagnetic performance of FSPM machines, as evidenced in the literature. For instance, a 6/17 FSPM machine with V-shaped stator pole demonstrated low cogging torque and ripple [22]. Additionally, an in-wheel FSPM motor based on V-shaped magnet placement was proposed, highlighting its superior torque capability and efficiency [23]. Another innovation involved a sandwiched FSPM machine with V-shaped magnet placement, leading to increased output torque and improved magnet usage efficiency through slot area enlargement [24].

Recently, the electromagnetic performance of a V-shaped FSPM machine was improved using a stepwise technique, which resulted in high power density and low cogging torque compared to the initial structure [25]. The outstanding features of the V-shaped FSPM motor have been revealed to enhance the power and torque capabilities of PM machines through an improved flux-focusing effect. As a result, this structure indicates high potential to be used for railway applications. Therefore, this work represents the first implementation of GA in V-shaped FSPM machines, which was targeted to enhance electromagnetic performance and achieve higher torque density, with a particular focus on optimizing the output torque for railway applications.

2. Traction motor topology

This study focuses on a motor topology specifically designed for railway traction. The benchmark motor topology, namely, a V-shaped FSPM motor, is illustrated in Figure 1(a) [25]. This motor design features a stator core with 12 slots, incorporating V-shaped segments positioned between two PMs installed in the stator pole with opposing polarities. The V-shaped flux-focusing magnet is designed to achieve high-power density for the FSPM motor. To enhance fault-tolerant capability, a 6-phase concentrated armature winding configuration is employed in this topology. Additionally, the optimal rotor with 19 poles and the optimal size for design variables, previously determined through a stepwise design approach, are incorporated to achieve a balance between efficient magnetic flux storage and manageable flux leakage. This optimized design technique results in higher power density. Figure 1(b) presents the optimal structure of the 6-phase V-shaped FSPM motor with adjusted design variables using the GA. The specific dimensions of both motors are detailed in Table 1, with design variables defined in Figure 2. Traction motors for railway applications demand high-output torque at high speeds. Consequently, the ratings and specifications of the V-shaped FSPM motor are outlined in Table 1.

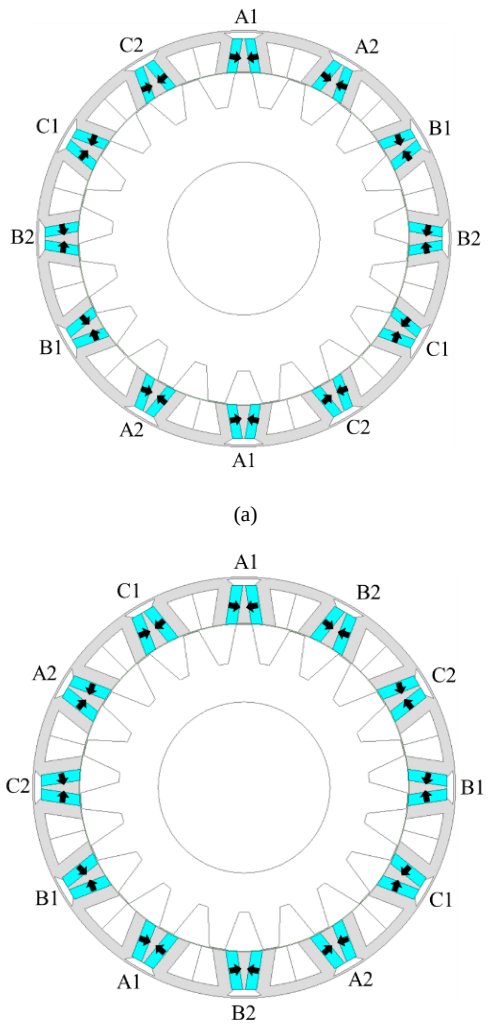

Fig. 1 (a) The initial and (b) the optimal structure of a 6-phase 12/19 V-shaped FSPM motor.

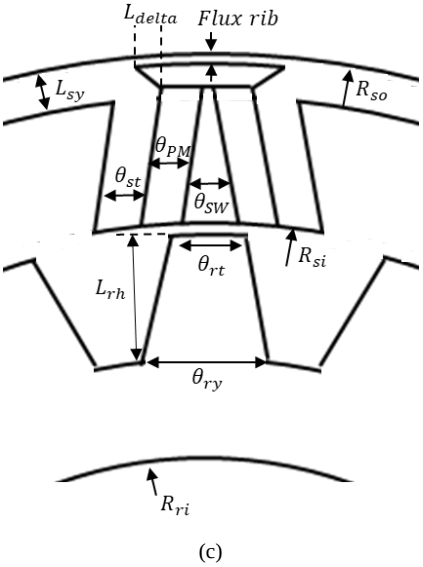

Fig. 2 2D-schematical design variables for the V-shaped FSPM motor.

Table 1 Dimension of V-shaped FSPM motor.

Parameters	Unit	Initial structure	Optimal structure
PM type	-	NdFeB	
Magnet remanence	T	1.2	
Magnet coercivity	kA/m	-909.46	
Axial length, L_s	mm	185	
Outer stator radius, R_{so}	mm	163.5	
Air gap length, g	mm	1	
Flux rib	mm	1.5	
Coil turn	turn	14	
Stator yoke length, L_{sy}	mm	8.56	8.08
Stator inner radius, R_{si}	mm	130.8	127.46
Cut delta, L_{delta}	degree	57.05	50.4
Stator pole width, θ_{st}	mm	9.2	10.12
PM width, θ_{PM}	mm	7.68	8.75
Rotor pole height, L_{rh}	mm	25.96	29.61
Rotor inner radius, R_{ri}	mm	60	66.36
Sandwiching pole arc, θ_{sw}	degree	4.92	4.94
Rotor pole width, θ_{rt}	mm	13.66	12.4
Rotor pole-yoke width, θ_{ry}	mm	24.63	24.48

Table 2 Ratings and specification of the V-shaped FSPM motor

Parameters	Value
Base speed (rpm)	2000
DC link voltage (V)	1500
Rated current (A_{rms})	100

3. Optimal design of the V-shaped FSPM motor

In the process of determining the design variables for FSPM motors, the initial dimensions of the proposed motor are obtained. To provide a clear and structured representation, the outlined comprehensive optimization procedure for the V-shaped FSPM motor is presented in Figure 3. This procedure encompasses several sequential steps as follows:

Firstly, the initial design phase of the V-shaped FSPM motor is conducted. During this stage, the requirements specific to railway applications and establish the optimization objectives are defined.

Secondly, the design variables and constraints are selected to formulate the motor's parametric model. To accomplish this, sensitivity analysis methods are employed to align the sensitivity indices of design variables with respect to the optimization objective. This aim in determine the boundaries of design variables for the subsequent optimization phase.

Thirdly, based on the above sensitivity analysis, the GA optimization method is applied to fulfill the predefined design requirements effectively.

Finally, the motor's performance is simulated, and a comparative analysis is conducted before and after optimization. This analysis serves to validate the proposed V-shaped FSPM motor and assess the effectiveness of the optimization methodology.

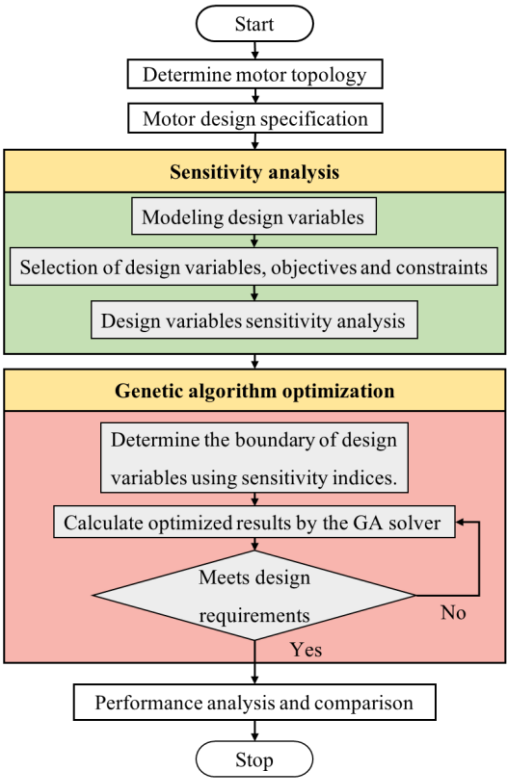

Fig. 3 Flowchart of the FSPM design variable sizing process.

3.1 Sensitivity analysis

To enhance the subsequent optimization process, this study incorporates sensitivity analysis. The purpose of sensitivity analysis is to assess the impact of design parameters on the output torque, thereby prioritizing their influence. The sensitivity index, S_i can be calculated as:

$$S_i = \frac{F(X_0 \pm \Delta X_i) - F(X_0)}{\pm \Delta X_i} \quad (1)$$

Where $F(X)$ represents the objective function, X_0 denotes the initial value, and X_i corresponds to the value of the design variables, $\pm \Delta X_i$ is typically defined as 10% or 20% of its initial value.

As depicted in Figure 4, a sensitivity analysis of the ten design variables is conducted. The sensitivity value indicates the degree of correlation between the optimization objective and each dimensional variable, with positive and negative values signifying positive and negative correlations, respectively. Notably, the stator inner radius, sandwiching pole arc, stator pole width, and PM width significantly influence the output torque. Observably, changes in the size of the stator's inner radius impact other design variables, leading to a high sensitivity value. Meanwhile, the negative sensitivity value indicates that an increase in the stator's inner radius results in a reduction in output torque. Furthermore, the sensitivity analysis allows for the clear ranking of design variables based on their

sensitivity index values from greatest to least, as illustrated in Table 3. This ranking of design variables will be utilized to define parameter boundaries for the GA optimization, as explained in the subsequent section.

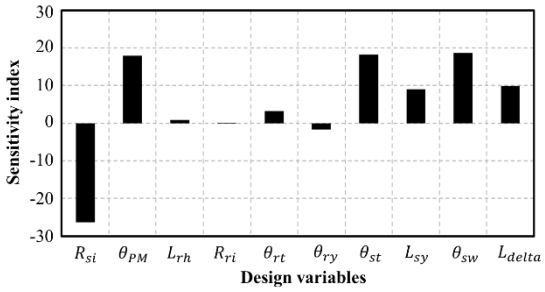

Fig. 4 Sensitivity analysis for the output torque.

Table 3 Sensitivity values of design variables

Design variables	Objective
	Output torque
Stator inner radius, R_{si}	-26.2677
Sandwiching pole arc, θ_{sw}	18.7153
Stator pole width, θ_{st}	18.1579
PM width, θ_{PM}	17.9343
Cut delta, L_{delta}	9.9391
Stator yoke length, L_{sy}	9.0659
Rotor pole width, θ_{rt}	3.2636
Rotor pole-yoke width, θ_{ry}	-1.6490
Rotor pole height, L_{rh}	0.8266
Rotor inner radius, R_{ri}	0.1777

3.2 Parameter optimization design

To facilitate the subsequent design optimization process, the initial values and variation ranges of the design variables are compiled, as detailed in Table 4. These values play a significant role in optimizing the torque performance through GA optimization. It's important to emphasize that the boundaries for each design variable are established based on the sensitivity analysis ranking. As a result, the selected normal design boundaries for these design variables aim to ensure the maximum output torque of the motor. To provide a comprehensive view of the optimization process, The results in Figure 5 indicate that, after nearly 400 generations of GA optimization, the process successfully converges to the optimal solution. This visualization illustrates the achievement of the optimization goal. This convergence represents a noteworthy transformation in the motor's structure as part of the endeavor to enhance output torque and accomplish the optimization objectives.

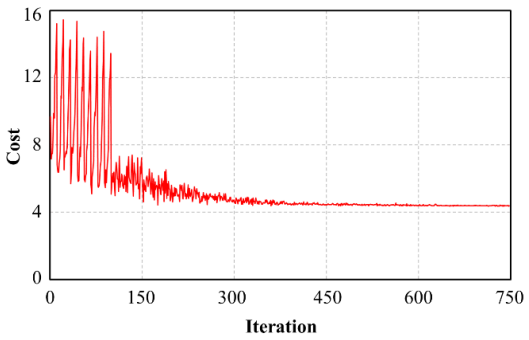

Fig. 5 The trajectory of the objective function value changes with the number of iterations in GA.

Table 4 Initial values, boundaries, and optimal values of design variables.

Design variables	Unit	Initial values	Boundaries	Optimal values
R_{si}	mm	130.8	124.3-137.3	127.46
θ_{sw}	degree	4.92	7.8-11.7	4.94
θ_{st}	mm	9.2	7.1-10.7	10.12
θ_{PM}	mm	7.68	6-9.1	8.75
L_{delta}	degree	57.05	45-70	50.4
L_{sy}	mm	8.56	6.8-10.3	8.08
θ_{rt}	mm	13.66	10.8-16.4	12.4
θ_{ry}	mm	24.63	15.5-34.8	24.48
L_{rh}	mm	25.96	20.7-31.2	29.61
R_{ri}	mm	60	48-72	66.36

4. Electromagnetic performance analysis

4.1.1 PM flux line distribution

Figure 6 compares the distributions of flux lines between the initial structure and the optimal structure of the 6-phase V-shaped FSPM motor. It's evident that all the design variables have been adjusted to suitable sizes, aligning with the optimized results from the GA analysis aimed at enhancing the motor's output torque. This clearly demonstrates the expansion of the area for inducing EMF, specifically involving design variables with a high sensitivity index. These variables include the stator's inner radius, the sandwiching pole arc, stator pole width, and PM width. These adjustments have resulted in an increased generation of effective flux, consequently leading to a substantial enhancement in output torque production. Furthermore, the optimal structure stands out with the most intense distribution of PM flux lines across rotor pole sections. This difference is attributed to a critical factor - an increase in the PM volume. This optimized design technique implies a higher power density in the 6-phase V-shaped FSPM motor, which has the potential to significantly enhance overall performance.

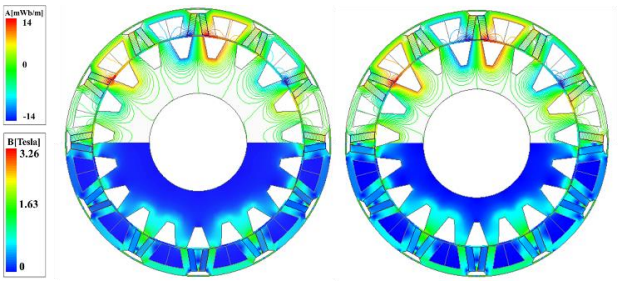

Fig. **6** PM flux distributions of V-shaped structure. (a) Initial structure (b) Optimal structure.

4.1.2 Back-EMF

Figures 7(a) and 7(b) illustrate the waveforms and spectra of the open-circuit phase back-EMF for both motors, respectively. It is evident that the optimal motor structure generates a higher phase back-EMF compared to the initial design. This improvement is primarily attributed to a more balanced distribution of magnetic flux paths within the machine. The magnetic flux circulates more uniformly across the machine thanks to the appropriate sizing of all design variables. This leads to better utilization of the generated magnetic field and, consequently, a higher phase back-EMF. Specifically, the optimal structure produces a phase back-EMF of up to 471 V_{rms}, which is 10.6% higher than that of the initial structure. However, it's worth noting that the optimal structures exhibit a higher total harmonic distortion (THD) value of 2.9% compared to the initial design (1.7%). This increase in THD can be attributed to operating closer to the saturation point of the magnetic circuit, introducing non-linearities in the magnetic behavior and resulting in a higher harmonic content in the phase EMF waveform.

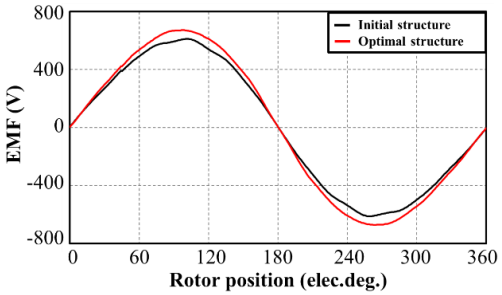

(a)

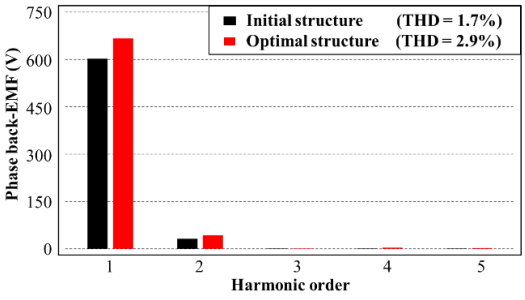

(b)

Fig. **7** Open-circuit phase back-EMF. (a) Waveforms (b) Spectrum.

4.1.3 Output torque

Figure 8 presents a comparison of the output torque characteristics between the initial and optimal motor structures, both operating under the same motor ratings and specifications (2000 rpm, 100 Arms). The results demonstrate that the optimal motor structure achieves significantly higher torque performance, yielding a remarkable output torque of up to 550 N·m. This represents a substantial increase of 9.3% when compared to the initial motor structure. The notable improvement in torque performance can be directly attributed to precise adjustments made to the dimensions of the design variables. These dimensions play a critical role in guiding magnetic circulation within the motor, allowing for accurate control and positioning. This enhanced control results in greater efficiency in torque production by maximizing the utilization of the magnetic field. Furthermore, the optimal structure exhibits a modest reduction in torque ripple in contrast to the initial design. This reduction in torque ripple highlights the precision with which the optimal structure leverages its design variables to minimize undesirable fluctuations in output torque. This controlled and smoother torque delivery is a crucial attribute that can significantly enhance the operational stability and performance of railway traction motors. It should be noted that the output torque of the proposed motor is at a commendable level when compared to other traction motors [26]-[33]. It contributes to a more reliable and efficient railway system.

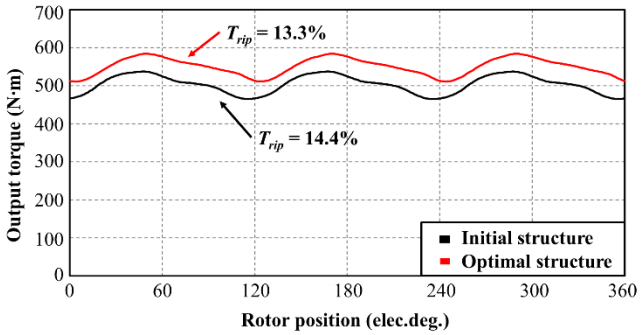

Fig. 8 Output torque waveforms

4.1.4 Efficiency

Table 5 compares performance indicators for the V-shaped FSPM motor. Impressively, the optimized V-shaped FSPM motor shows a remarkable 10.6% increase in output power compared to the initial structure, reaching an impressive 141.3 kW. This improvement is achieved by resizing design variables to enhance suitability, resulting in higher flux density and improved flux circulation. A lightly enhanced level of core losses is observed, primarily attributed to the comparatively higher flux densities. Additionally, a slightly larger PM usage contributes to a minor enhancement in eddy current losses. Copper loss remains nearly unchanged from the initial setup, as the slot area is not significantly altered. It's crucial to clarify that, in this study, electrical losses are exclusively considered in

efficiency calculations. Despite these factors, the overall performance of the optimized structure is not compromised, achieving an impressive 93.4%. This ensures that the optimized V-shaped FSPM motor is suitable for use in railway traction motors.

Table 5 Comparison of performance indicators for the V-shaped FSPM motor.

Parameters	Unit	Initial structure	Optimal structure
phase back- EMF (rms)	V	425.9	471
Phase current (rms)	A	100	
Output power	kW	127.7	141.3
Average torque	N·m	503.4	550.2
Torque ripple factor	%	14.4	13.3
Copper loss	W	364.5	363.5
Core loss	W	3105.9	3402.9
PM-eddy current loss	W	2510.1	2743.1
Total loss	W	5980.5	6509.5
Efficiency	%	93.3	93.4

5. Conclusion

This study proposes the optimization design of a 6-phase V-shaped FSPM motor. The primary objective was to enhance electromagnetic performance and achieve higher torque density, with a specific emphasis on optimizing traction force for railway applications. By incorporating the GA optimization method, the accuracy of the optimal results was significantly enhanced by determining the boundaries of design variables through sensitivity index ranking. The study thoroughly investigates and compares the electromagnetic performance of the 6-phase V-shaped FSPM motor before and after the design optimization process. Following optimization, notable improvements were observed, including a 10.6% increase in phase back-EMF, a substantial 9.3% rise in average output torque, and a commendable 1.1% reduction in torque ripple. These enhancements collectively contribute to the development of a more reliable and efficient railway system. This work emphasized the potential of advanced optimization techniques in the field of railway traction motors.

References

[1] M. J. Hapeman, J. Long, and D. L. Plette, "Diesel electric locomotive propulsion systems—A look into the future," *IEEE Transactions on Industry Applications*, vol. IA-22, no. 3, pp. 495–501, May 1986.

[2] M. C. Duffy, *Electric Railways 1880-1990*, London, U.K.: The Institution of Engineering and Technology, 2003.

[3] R. J. Kemp, "Developments in electric traction," *Power Engineering Journal.*, vol. 3, no. 2, pp. 71–82, Mar 1989.

[4] M. C. Duffy, "Three-phase motor in railway traction," *IEE Proceedings A (Science, Measurement and Technology)*, vol. 139, no. 6, pp. 329–337, Nov 1992.

[5] A. Steimel, "Electric railway traction in Europe," *IEEE Industrial Applications. Magazine.*, vol. 2, no. 6, pp. 6–17, Nov/Dec 1996.

[6] A. Steimel, *Electric Traction – Motive Power and Energy Supply, Basics and Practical Experience*, Munich, Germany: Oldenbourg Industrieverlag GmbH, 2003.

[7] D. Ronanki, S. A. Singh, and S. S. Williamson, "Comprehensive Topological Overview of Rolling Stock Architectures and Recent Trends in Electric Railway Traction Systems," *IEEE Transactions on Transportation Electrification*, vol. 3, pp. 724–738, May 2017.

[8] S.j. Rind, Y. Ren, Y. Hu, J. Wang, and L. Jiang, "Configurations and Control of traction Motors for Electric Vehicles: A Review," *Chinese Journal of Electrical Engineering*, vol. 3, pp. 1–17, Dec 2017.

[9] W. Sriwannarat, P. Khunkitti, A. Janon, and A. Siritaratiwat, "An improvement of magnetic flux linkage in electrical generator using the novel permanent magnet arrangement," *Polska Akademia Nauk. Instytut Fizyki PAN.*, vol. 3, no. 113, pp. 642-644, Mar 2018.

[10] A. M. El-Refaie, "Motors/generators for traction/propulsion applications: A review," *IEEE Vehicular Technology Magazine*, vol. 8, no. 3, pp. 90–99. Feb 2013.

[11] J. O. Estima, A. J. M. Cardoso, "Efficiency Analysis of Drive Train Topologies Applied to Electric/Hybrid Vehicles," *IEEE Transactions on Vehicular Technology*, vol. 61, no. 3, pp. 1021 - 1031, May 2017.

[12] W. Sriwannarat, P. Seangwong, V. Lounthavong, S. Khunkitti, A. Siritaratiwat, and P. Khunkitti, "An improvement of output power in doubly salient permanent magnet generator using Pole configuration adjustment," *Energies.*, vol. 13, no. 17, pp. 4588, Sep 2020.

[13] V. Lounthavong, W. Sriwannarat, A. Siritaratiwat, and P. Khunkitti, "Optimal stator design of doubly salient permanent magnet generator for enhancing the electromagnetic performance," *Energies.*, vol. 12, no. 16, pp. 3201, Aug 2018.

[14] W. Sriwannarat, A. Siritaratiwat, and P. Khunkitti, "Structural design of partitioned stator doubly salient permanent magnet generator for power output improvement," *Advances in Materials Science and Engineering.*, vol. 2019, pp. 1-8, Apr 2019.

[15] V. Torn, P. Seangwong, N. Fernando, A. Siritaratiwat, and P. Khunkitti, "Performance Improvement of Flux Switching Permanent Magnet Wind Generator Using Magnetic Flux Barrier Design," *Sustainability.*, vol. 15, no. 11, pp. 8867, Apr 2023.

[16] J. Zhang, M. Cheng, Z. Chen, and W. Hua, "Comparison of stator mounted permanent-magnet machines based on a general power equation," *IEEE Transaction Energy Conversions.*, vol. 24, no. 4, pp. 826–834, Dec. 2009.

[17] W. Zhao, M. Cheng, W. Hua, H. Jia, and R. Cao, "Back-EMF harmonic analysis and fault-tolerant control of flux-switching permanent-magnet machine with redundancy," *IEEE Transactions on Industrial Electronics*, vol. 58, no. 5, pp. 1926–1935, May 2011.

[18] D. Fu, K. Wu, P. Zheng, Q. Yu, and X. Wu, "Force Modeling and Analysis of a Tube Flux-Switching Transverse-Flux Permanent Magnet Linear Motor," *IEEE Transactions on Industry Applications*, vol. 58, no. 4, pp. 4575–4586, Jul/Aug 2022.

[19] I. Eguren, G. Almandoz, A. Egea, S. Zarate, and A. Urdangarin, "Thrust Ripple Reduction in Linear Switched-Flux Machines via Additional Pole Optimisation," *IEEE Transactions Energy Conversions*, vol. 37, no. 3, pp. 1655-1665, Sep 2022.

[20] B. Ullah, F. Khan, S. Hussain, and B. Khan, "Modeling, Optimization, and Analysis of Segmented Stator Flux Switching Linear Hybrid Excited Machine for Electric Power Train," *IEEE Transactions on Industrial Electronics*, vol. 8, no. 3, pp. 3546-3553, Sep 2022.

[21] S. Hussain, F. Khan, W. Ullah, B. Ullah, and B. Khan, "Optimization and Experimentation of Fault-Tolerant Field Excited Linear Flux Switching Machine with Concentrated and Toroidal Windings for Rail Transportation System," *IEEE Transactions on Industry Applications, vol.* 59, no. 2, pp. 1361-1371, Mar/Apr 2023.

[22] G. Zhao, and W. Hua, "Comparative Study between a Novel Multi-Tooth and a V-Shaped Flux-Switching Permanent Magnet Machines," *IEEE Transactions on Magnetics*, vol. 55, no. 7, pp. 1-8, Mar 2019.

[23] X. Zhu, Z. Shu, L. Quan, Z. Xiang, and X. Pan, "Design and Multi condition Comparison of Two Outer-Rotor Flux-Switching Permanent-Magnet Motors for in-Wheel Traction Applications," *IEEE Transactions on Industrial Electronics*, vol. 64, no. 8, pp. 6137 - 6148, Aug 2017.

[24] Y.J. Zhou, and Z.Q. Zhu, "Torque Density and Magnet Usage Efficiency Enhancement of Sandwiched Switched Flux Permanent Magnet Machines Using V-Shaped Magnets," *IEEE Transactions on Magnetics*, vol. 49, no. 7, pp. 3834 - 3837, July 2013.

[25] P. Seangwong, S. Chamchuen, N. Fernando, A. Siritaratiwat, and P. Khunkitti, "A Novel Six-Phase V-Shaped Flux-Switching Permanent Magnet Generator for Wind Power Generation," *Energies.*, vol. 15, no. 24, pp. 9608, Dec 2022.

[26] D. Yu, X.Y. Huang, Y.T. Fang and J Zhang, "Design and Comparison of Interior Permanent Magnet Synchronous Traction Motors for High-Speed Railway Applications," *IEEE WEMDCD.*, pp. 58–62, Jun 2017.

[27] P. Lindh, I. Petrov, and J. Pyrhönen, "Comparison of Halbach rotors with other PM structures" *IEEE IEMDC.*, pp. 721–726, May 2019.

[28] P-W Han, U-J Seo, S. Paul, and J. Chang, "Computationally Efficient Stator AC Winding Loss Analysis Model for Traction Motors Used in High-Speed Railway Electric Multiple Unit," *IEEE Access.* vol. 10, pp. 28725 - 28738, Mar 2022.

[29] J. Sobra, K. Hruska, and J. Laksar, "Analysis of Traction Permanent Magnet Motor with Static and Dynamic Eccentricities," *2020 International Conference on Electrical Machines (ICEM)*, pp. 1294 - 1300, Dec 2020.

[30] L. Boscaglia, N. Sharma, Y. Liu, and G. Mademlis, "Balancing Peak-torque and Drive-cycle Efficiency with Magnet Dimensioning of Permanent Magnet Synchronous Machines," *IECON 2020 The 46th Annual Conference of the IEEE Industrial Electronics Society*, pp. 883 - 888, Oct 2020.

[31] H. Jang, H. Kim, D.W. Nam, W.H. Kim, J. Lee, and C. Jin, "Investigation and Analysis of Novel Skewing in a 140 kW Traction Motor of Railway Cars That Accommodate Limited Inverter Switching Frequency and Totally Enclosed Cooling System," *IEEE Access.* vol. 9, pp. 121405 - 121413, Aug 2021.

[32] Y.J. Oh, H.-C. Liu, S. Cho, J. H. Won, H. Lee, and J. Lee, "Design, Modeling, and Analysis of a Railway Traction Motor with Independently Rotating Wheelset" *IEEE Transactions on Magnetics*, vol. 54, no. 11, pp. 8205305, Nov 2018.

[33] M. Degano, E. Carraro, and N. Bianchi, "Selection Criteria and Robust Optimization of a Traction PM-Assisted Synchronous Reluctance Motor," *IEEE Transactions on Industry Applications.*, vol. 51, no. 6, pp. 4383–4391, Nov.-Dec. 2015.